38th International Electric Vehicle Symposium and Exhibition (EVS38)
Göteborg, Sweden, June 15-18, 2025

Techno-Economic Optimization of PV and Battery for Airport Microgrids

Qian Xun, Patrik Ollas
Qian Xun (corresponding author) RISE Research Institutes of Sweden, Borås, Sweden, qian.xun@ri.se

Executive Summary

Photovoltaic (PV) systems are pivotal in facilitating the green energy transition within the aviation sector. However, due to the inherent intermittency of PV power generation and variable electricity tariffs from the utility grid, integrating battery energy storage systems (BESS) becomes essential to ensure optimal energy utilization. Since airports exhibit complex and variable electricity demand patterns, achieving optimal component sizing and efficient power allocation remains a significant challenge. This paper presents a co-design optimization framework aimed at concurrently determining the optimal sizing of PV and BESS, along with efficient power allocation strategies between the utility grid and the BESS. The framework comprehensively considers real-world scenarios, including airport operational demands and charging loads of electric aircraft and electric vehicles derived from flight schedules. The effectiveness and practical applicability of the optimization approach are validated through four case studies. The results provide valuable guidance for selecting appropriate component sizes and optimizing power allocation strategies for an airport microgrid application.

Keywords: Electric ships & airplanes, smart grid integration and grid management, modeling and simulation, energy management, sustainable energy.

1 Introduction

The COVID-19 pandemic resulted in a temporary decline in global aviation activities; however, emissions are projected to rebound as air travel resumes its growth trajectory. Before the pandemic, commercial aviation was responsible for emitting over 900 million metric tons of CO_2, marking an increase of approximately 627 million metric tons compared to 2004 [1]. Although pandemic-related travel restrictions led to a 60% reduction in aviation emissions in 2020, forecasts suggest emissions will rise to approximately 1.5 billion metric tons by 2050. Concurrently, aviation plays a pivotal role in urban development and economic growth [2]. To address the environmental concerns associated with increasing aviation emissions, renewable energy-powered electric aviation has emerged as a promising solution, especially for short-haul flights up to 1500 km.

Airports, characterized by extensive, flat, and obstacle-free land areas, offer ideal conditions for deploying large-scale solar photovoltaic (PV) systems. Integrating renewable energy into airport operations has been recognized as a crucial sustainability strategy [3]. Several significant initiatives have been implemented, such as the project at Rome Fiumicino Airport project, aiming to establish the largest self-consumption solar farm in Europe [4], and the testing facility at the Hannover Airport, which explores agricultural practices beneath PV installations [5]. On-site PV generation provides numerous benefits, including reduced dependency on the grid, lower operational expenses, and mitigation of peak power demands. A comprehensive study focusing on Chinese airports [6] estimated that 239 airports collectively

possess a potential PV capacity of 2.5 GW, generating approximately 2.65 TWh annually. Nevertheless, this study underscores the importance of incorporating energy storage systems (ESS) to improve the temporal alignment between PV generation and energy consumption patterns of airports.

Battery-powered aircraft are anticipated to constitute a significant portion of short-haul flights [7], considerably affecting airport energy infrastructure by introducing substantial peak power demands [8]. Due to the required battery capacities and short turnaround times, the peak power demands reach megawatt-scale levels [9]. Although grid capacity expansion offers a viable solution, it involves significant capital investments and prolonged development timelines. Battery energy storage systems (BESS) have emerged as an effective alternative to address these challenges by mitigating peak load impacts and enhancing overall grid stability [10]. Existing BESS implementations at airports, including those at Copenhagen Airport in Denmark [11] and Schiphol Airport in the Netherlands [12], have demonstrated the practicality and effectiveness of such approaches.

Despite growing interest in airport energy systems, the integration of microgrids within airports remains relatively underexplored [13], with only a limited number of studies addressing techno-economic feasibility [10, 14, 15]. In [14], a mixed integer linear programming (MILP) is employed to optimize the techno-economic performance of five energy configuration scenarios at an airport. The referred work includes PV, BESS, and hydrogen storage but excludes electric aircraft (EA) demand. The work in [16] uses MILP for a techno-economic and resilience airport evaluation but excludes the airport load demand. Both of these studies [14, 16] employed single-objective battery operations, and previous works, e.g., [17, 18] highlighted limitations associated with single-objective operation and proposed multi-objective strategies to exploit BESS potential fully. Ollas et al. [10] conducted a comprehensive techno-economic assessment of a regional airport in Sweden, integrating PV and BESS systems. They compared rule-based BESS dispatch strategies, examining both single-objective and revenue-stacking operations, with particular attention to battery aging effects. This study evaluated three distinct PV system designs and system sizing to maximize power generation based on available locations. However, BESS sizing was primarily assessed through the single metric of self-consumption.

A key challenge remains in identifying optimal sizing for PV and BES components while balancing on-site energy generation and grid interactions to minimize investment and operational costs. To address this, this paper introduces a co-design optimization framework for optimal sizing and energy management of the airport energy system. The proposed methodology is applied to a case study at Visby Airport, Sweden, where four energy scenarios are analyzed. The results offer critical insights for optimizing renewable energy and storage configurations tailored to airport applications.

The remainder of this paper is structured as follows. Section 2 describes the configuration of the investigated energy infrastructure and details the modeling of system components. Section 3 provides the mathematical formulation of the optimization problem. Section 4 presents the case study, and Section 5 discusses the simulation results. Finally, Section 6 outlines the conclusions.

2 System Architecture and Model Development

Fig. 1 illustrates the comprehensive energy infrastructure designed for the airport microgrid. The PV system, the grid, and the BESS provide electric power. The load power demand encompasses various airport facilities, including terminal buildings, runway lighting, air traffic control towers, ground support equipment, and charging infrastructure for EA and EV. To simplify the system representation, the efficiencies of power converters are not considered, and thus, power converters are omitted from Fig. 1. The power demand (p_{ld}) represents an aggregated load consumption, summarizing the combined consumption of all electric consumers within the airport. Consequently, the power balance equation is expressed as

$$p_{\mathrm{pv}}(t) + p_{\mathrm{bt}}(t) + p_{\mathrm{gdb}} + p_{\mathrm{gds}}(t) + p_{\mathrm{curtail}}(t) \equiv p_{\mathrm{ld}}(t), \tag{1}$$

where p_{pv} denotes the output power from the PV system, p_{bt} represents the terminal power of the BESS, p_{gdb} is the imported power from the grid, p_{gds} is exported power to the grid and p_{curtail} signifies the curtailed PV power when p_{gds} reaches its allowable limit. Here, the power imported from the grid p_{gdb} is constrained to be non-negative, whereas the exported grid power p_{gds} and p_{curtail} are non-positive. The grid power interaction in (1) is limited by the nominal capacity of the transformer ($\mathrm{P_{tr}}$), expressed as

$$0 \leqslant p_{\mathrm{gdb}}(t) \leqslant \mathrm{P_{tr}}, \tag{2}$$

$$-\mathrm{P_{tr}} \leqslant p_{\mathrm{gds}}(t) \leqslant 0. \tag{3}$$

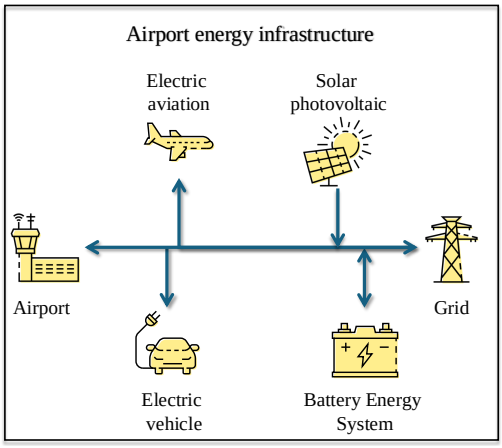

Figure 1: Schematic layout of the airport energy infrastructure.

2.1 PV Model

The output power of the PV systems significantly depends on geometric parameters (e.g., module dimensions), installation tilt angles, and meteorological conditions, such as solar irradiation, ambient temperature, and air mass coefficient. Since individual PV cells or modules typically produce relatively low voltage and current, modules are often interconnected in series and parallel configurations to achieve the desired system-level voltage and power outputs. Therefore, the total PV array output can be modeled as a scaled version of a baseline PV module. The baseline module output is often estimated using empirical models derived from experimental data or simulations conducted with specialized PV modeling software [19, 20]. Mathematically, the scaled PV system output can be expressed as

$$p_{\mathrm{pv}}(t)' = s_{\mathrm{pv}} p_{\mathrm{pv}}(t) \tag{4}$$

where $p_{\mathrm{pv}}(t)$ is the reference power profile from the baseline module, and s_{pv} is a scaling factor subjected to the following constraints

$$s_{\mathrm{pv}}^{\min} \leqslant s_{\mathrm{pv}} \leqslant s_{\mathrm{pv}}^{\max}, \tag{5}$$

with $s_{\mathrm{pv}}^{\min}$ and $s_{\mathrm{pv}}^{\max}$ representing the minimum and maximum permissible scaling factors, respectively.

2.2 Battery Model

The battery cell is represented as a controlled voltage source in series with an internal resistor. A battery pack comprises n_{b} cells arranged in series and parallel configurations. The terminal power of the battery pack is described as

$$p_{\mathrm{btb}}(t) = \left(u_{\mathrm{b}}(t) i_{\mathrm{b}}(t) - \mathrm{R}_{\mathrm{b}} i_{\mathrm{b}}^2(t)\right) n_{\mathrm{b}} \tag{6}$$

where $i_{\mathrm{b}}(t)$ denotes the cell current, R_{b} the internal resistance, and $u_{\mathrm{b}}(t)$ is the open-circuit voltage (OCV), which is dependent on the state of charge (SoC). Within a certain SoC operating range, the OCV can be approximated as [21]

$$u_{\mathrm{b}}(t) = a_0 \mathrm{soc}_{\mathrm{b}}(t) + a_1 \tag{7}$$

where a_0 and a_1 are empirical fitting coefficients, and $\mathrm{soc}_{\mathrm{b}}(t)$ represents the battery SoC. The stored energy within the battery pack can be expressed as

$$e_{\mathrm{bb}}(t) = \frac{n_{\mathrm{b}} \mathrm{C}_{\mathrm{b}}}{2} \left(u_{\mathrm{b}}^2(t) - u_{0\mathrm{b}}^2\right). \tag{8}$$

Consequently, the terminal power can be reformulated as

$$p_{\mathrm{btb}}(t) = p_{\mathrm{bb}}(t) - \frac{\mathrm{R}_{\mathrm{b}} \mathrm{Q}_{\mathrm{b}} p_{\mathrm{bb}}^2(t)/a_0}{2e_{\mathrm{bb}}(t) + a_1^2 \mathrm{Q}_{\mathrm{b}} n_{\mathrm{b}}/a_0}, \tag{9}$$

where $p_{\mathrm{bb}}(t)$ denotes the internal power of the battery pack, and Q_{b} represents the rated capacity of the battery cell. Similar to the PV system model, the scaled version of the battery pack energy and power are given by

$$e_{\mathrm{b}}(t) = s_{\mathrm{b}} e_{\mathrm{bb}}(t) \tag{10}$$

$$p_{\mathrm{b}}(t) = s_{\mathrm{b}} p_{\mathrm{bb}}(t) \tag{11}$$

where s_{b} is the scaling factor. The dynamics governing the battery pack energy state are described by

$$\dot{e}_{\mathrm{b}}(t) = -p_{\mathrm{b}}(t). \tag{12}$$

The battery operates as a daily energy buffer, completing a full charge-discharge cycle each day to maintain daily energy balance. This can be mathematically expressed as

$$E_{\mathrm{b}}^{1}(1) = E_{\mathrm{b}}^{k}(1), \quad k \in \{2, 3, ..., N, N+1\}, \tag{13}$$

where $E_{\mathrm{b}}^{1}(1)$ and $E_{\mathrm{b}}^{k}(1)$ represent the battery internal energy at the initial time sample of the first day and the k-th day, respectively, with N representing the number of days in a year. The power and energy of the battery pack must be maintained within physical operational constraints. These constraints, along with the scaling factor, are defined as follows

$$\mathrm{P}_{\mathrm{b}}^{\min} \leqslant p_{\mathrm{b}}(t) \leqslant \mathrm{P}_{\mathrm{b}}^{\max}, \tag{14}$$

$$\mathrm{E}_{\mathrm{b}}^{\min} \leqslant e_{\mathrm{b}}(t) \leqslant \mathrm{E}_{\mathrm{b}}^{\max}, \tag{15}$$

$$s_{\mathrm{b}}^{\min} \leqslant s_{\mathrm{b}} \leqslant s_{\mathrm{b}}^{\max}, \tag{16}$$

where $\mathrm{P}_{\mathrm{b}}^{\min}$, $\mathrm{P}_{\mathrm{b}}^{\min}$, $\mathrm{E}_{\mathrm{b}}^{\min}$, $\mathrm{E}_{\mathrm{b}}^{\min}$, $s_{\mathrm{b}}^{\min}$, and $s_{\mathrm{b}}^{\max}$ represent the lower and upper bounds for battery power p_{b}, battery energy e_{b}, and scaling factor s_{b}, respectively.

3 Problem Formulation

3.1 Objective Function

The objective function aims to minimize total system costs, encompassing investment (PV and BESS), operating (electricity and maintenance), and CO_2 emission costs. Investment costs are upfront, whereas operating and CO_2 costs recur continuously. Hence, all costs element are normalized to €/day for comparative purposes [21].

The investment cost can be expressed as

$$\mathbb{C}_{\mathrm{inv}} = \left(\frac{\beta_{\mathrm{pv}} \mathrm{P}_{\mathrm{pv}}^{\mathrm{nom}}}{y_{\mathrm{y}} y_{\mathrm{d}}} + \frac{s_{\mathrm{b}} n_{\mathrm{b}} \mathrm{Q}_{\mathrm{b}} \beta_{\mathrm{b}}}{y_{\mathrm{y}} y_{\mathrm{d}}} \right) \mathrm{CF} \tag{17}$$

where β_{pv} and β_{b} represent the unit investment costs for PV and BESS, respectively. $\mathrm{P}_{\mathrm{pv}}^{\mathrm{nom}}$ is the nominal power of the PV system, and Q_{b} is the nominal capacity of the battery. The terms y_{y} and y_{d} denote the system lifespan and the average annual service days, respectively. The cost factor (CF), related to the interest rate, is calculated as

$$\mathrm{CF} = 1 + p_{\mathrm{y}} \frac{n_{j,\mathrm{r}} + y_{\mathrm{r}} + 1}{2(n_{j,\mathrm{r}} + 1)}, \tag{18}$$

where p_{y} is the annual interest rate, and $n_{j,\mathrm{r}}$ represents the number of replacements required for component j (where $j \in \{\mathrm{pv}, \mathrm{b}\}$) during the airport service operational lifetime.

The operating cost includes electricity import and export charges, peak power surcharges, and maintenance expenses, described as

$$\begin{aligned} \mathbb{C}_{\mathrm{opt}} = \frac{1}{y_{\mathrm{d}}} \Bigg(& \int_{t_0}^{t_{\mathrm{f}}} \beta_{\mathrm{eleb}}(t) p_{\mathrm{gdb}}(t)\, \mathrm{d}t + \int_{t_0}^{t_{\mathrm{f}}} \beta_{\mathrm{eles}}(t) p_{\mathrm{gds}}(t)\, \mathrm{d}t \\ & + \sum_{j} \beta_{j}^{\mathrm{O\&M}} \Phi_j + \beta_{\mathrm{peak}} \sum_{m=1}^{12} p_{\mathrm{gdb}}^{\max}\left(t(m)\right) \Bigg), \end{aligned} \tag{19}$$

where time-dependent electricity tariffs for importing (β_{eleb}) and exporting (β_{eles}) power are applied. The maintenance cost ($\beta_{j}^{\mathrm{O\&M}}$) is proportional to the rated capacity (Φ_j) of each component, and β_{peak}

denotes the monthly peak power surcharge, determined by the highest hourly power demand of each month. The term m indicates the respective month.

The CO_2 emission cost, based on grid electricity consumption, is calculated as

$$\mathbb{C}_{\mathrm{co_2}} = \frac{\beta_{\mathrm{co_2}} c_{\mathrm{co_2}}}{y_{\mathrm{d}}} \int_{t_0}^{t_{\mathrm{f}}} p_{\mathrm{gdb}}(t)\mathrm{d}t, \tag{20}$$

where $\beta_{\mathrm{co_2}}$ represents the carbon tax, and $c_{\mathrm{co_2}}$ denotes the carbon emission factor from the grid electricity.

Thus, the comprehensive cost minimization objective function, including (17)–(20), is formulated as

$$J(\mathbf{d}, \mathbf{x}(t), \mathbf{u}(t), \mathbf{p}) = \mathbb{C}_{\mathrm{inv}} + \mathbb{C}_{\mathrm{opt}} + \mathbb{C}_{\mathrm{co_2}}, \tag{21}$$

where $\mathbf{d} = [s_{\mathrm{pv}},\ s_{\mathrm{b}}]$ are the decision variables, $\mathbf{u}(t) = [p_{\mathrm{b}}(t),\ p_{\mathrm{gdb}}(t),\ p_{\mathrm{gds}}(t)]$ represent the control variables, and $\mathbf{x}(t) = [e_{\mathrm{b}}(t)]$ denotes the state variable. Due to the complexity, the parameter vector $\mathbf{p}(t)$ is extensive and thus not explicitly listed.

3.2 Optimization Problem

The formulated problem can be compactly expressed as follows,

$$\min_{\mathbf{d},\ \mathbf{x}(t),\ \mathbf{u}(t)} J\left(\mathbf{d}, \mathbf{x}(t), \mathbf{u}(t), \mathbf{p}\right), \tag{22}$$

with respect to the inequality constraint

$$\mathbf{h}(\mathbf{d}, \mathbf{x}(t), \mathbf{u}(t), \mathbf{p}(t), t) \leqslant 0, \tag{23}$$

the equality constraint

$$\mathbf{g}(\mathbf{d}, \mathbf{x}(t), \mathbf{u}(t), \mathbf{p}(t), t) = 0, \tag{24}$$

and system dynamics

$$\dot{\mathbf{x}}(t) - \mathbf{f}(\mathbf{d}, \mathbf{x}(t), \mathbf{u}(t), \mathbf{p}(t), t) = 0. \tag{25}$$

The inequality constraint (23) encompasses constraints (2), (3), (5), (14)–(16), while the equality constraint (24) includes (13). The system dynamics constraint involves (12). To simplify the calculation of the curtailed PV power in (1), this equality constraint is relaxed into an inequality, expressed as

$$P_{\mathrm{pv}}(t) + P_{\mathrm{bt}}(t) + P_{\mathrm{gdb}} + P_{\mathrm{gds}}(t) \geqslant P_{\mathrm{ld}}(t), \tag{26}$$

which is incorporated within the inequality constraint (23).

4 Case Study and Main Specifications

The Visby airport on the island of Gotland, Sweden is analyzed as a case study using the airport energy demand, and EA and electric vehicles (EV) charging demands from [10]. The EV demand is generated considering flight schedules (16 departures per day), parking patterns, and site-specific parameters, and with the EA demand model from [22]. Fig. 2(a) and Fig. 2(b) show the EA charging demand per hour and day of the year. The introduction of EA significantly increases the peak power demand at the airport. In the same way, Fig. 2(b) shows the EV demand distributions. The airport demand in Fig. 2(c) is acquired from hourly measurements 2018. Fig. 2(d) shows the superimposed demands, with peak powers originating from the EA demand. The electricity price for bought and sold electricity, β_{eleb} and β_{eles} in (19), is taken as the hourly values from the NordPool market, including VAT and other charges [10].

Four operating scenarios are examined to evaluate the techno-economic viability of various energy configurations for airport microgrid applications, with Case 1 serving as the reference scenario. The scenarios are detailed as follows:

Case 1: No PV or BESS installed and all power demands are met by the utility grid,

Case 2: PV system is implemented to reduce operating costs, with surplus generated energy sold back to the grid,

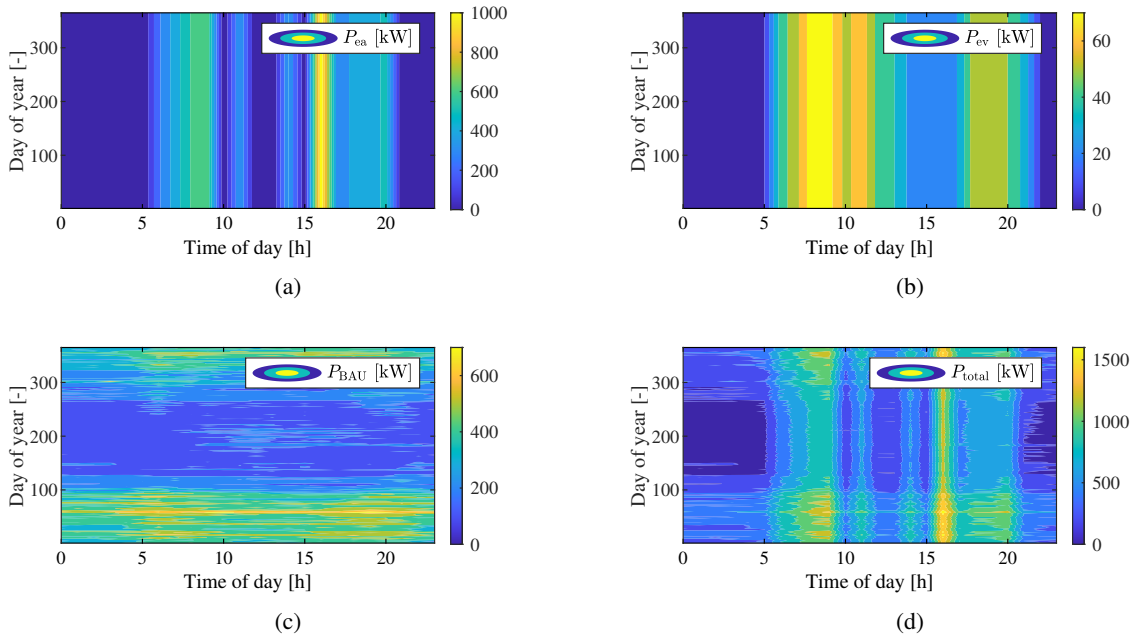

Figure 2: Contour plots of load demands per daily hour and day of the year for the case study, showing **(a)**: EA, **(b)**: ground service EV, **(c)**: airport, and **(d)**: combined airport, EA, and ground service EV demand.

Case 3: BESS is deployed to facilitate energy arbitrage and peak shaving, and

Case 4: Both PV and BESS are installed, optimizing energy management with the grid, and excess electricity generation is sold.

For all cases, the nominal capacity of the grid transformer (P_{tr}) is set to handle the peak power from the aggregated demand (1.8 MW), as per Fig. 2(d). This also means 1.8 MW allowed power to be sold back to the power grid. The PV output of the baseline module in (4) is taken from the ground-mounted array in Location 1 from [10], and the parameters of the baseline battery cell are taken from [23]. The techno-economic parameters are retrieved from [14] and shown in Table 1.

Table 1: Main parameters used for case study [14].

Investment & maintenance	Component	Capital cost, β_j	Maintenance cost, $\beta_j^{O\&M}$ [€/year]	Lifetime [year]
	PV	545 €/kW	8 €/kW	25
	Battery	100 €/kWh	5 €/kWh	10
Other parameters	Parameter [Unit]			Value
	Peak power tariff, β_{peak} [€/kW]			4.5
	Carbon tax, β_{co_2} [€/kg]			1.34×10^{-1} [24]
	Carbon emission factor, c_{co_2} [kg/kWh]			1.8×10^{-2} [25]
	Airport annual service period, y_d [day]			365
	Airport average service year, y_y [year]			25
	Yearly interest rate, p_y [-]			5%

5 Simulation Results

5.1 Optimal Sizing of PV and battery Systems

This section presents the optimal sizing results of PV and battery energy systems analyzed through four case studies, each featuring distinct configurations of PV and battery systems. Table 2 summarizes the

Table 2: Optimal PV (P_{pv}^{nom}) and battery (Q_b) sizing for the four cases, and associated total costs ($\mathbb{C}_{tot}$).

	P_{pv}^{nom} [MW]	Q_b [MWh]	$\mathbb{C}_{tot}$ [€/day]	Self-sufficiency rate [%]
Case 1	–	–	2019	0
Case 2	3.6	–	1174	33
Case 3	–	0.98	1964	0
Case 4	3.6	2.8	1082	41

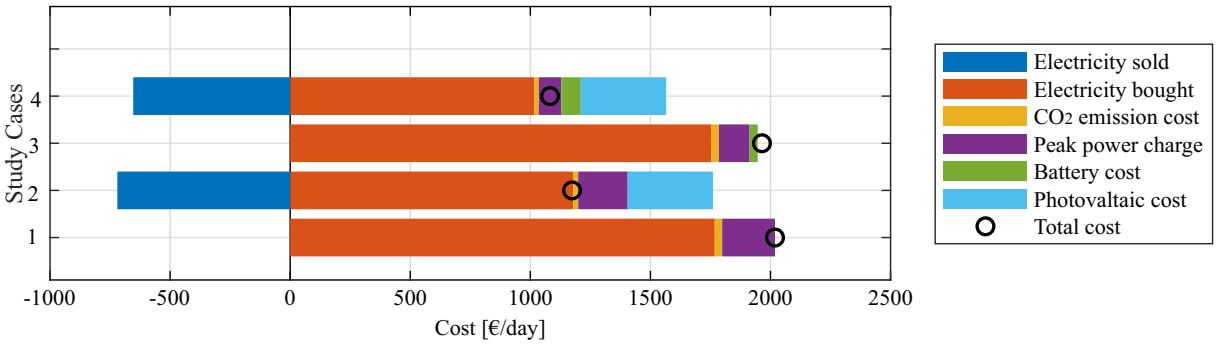

Figure 3: Cost composition breakdown for each case.

optimal PV power ratings, battery energy capacities, and associated total costs. The results indicate that Case 2 and Case 4 yield identical optimal PV capacities, reaching the upper limit imposed by the maximum allowable power grid capacity (P_{tr}) of 1.8 MW. It is anticipated that the optimal PV capacity could further increase if P_{tr} increases.

Comparing Cases 3 and 4, the battery energy capacities exhibit significant differences, with Case 4 showing a higher capacity due to the involvement of the PV system. Regarding total costs, Case 4 demonstrates the most significant economic advantage, achieving a cost reduction of 46% compared to Case 1. This finding underscores the financial benefit of simultaneously integrating PV and battery systems. Case 2, with only PV, ranks second in terms of cost-effectiveness, primarily due to the initial capital expenditure of PV panels being offset by subsequent electricity generation without additional operational costs. Case 3 results in a marginal cost reduction of merely 2.69% relative to Case 1. This modest reduction can be attributed to minimal daily fluctuations in electricity pricing, limiting the battery potential to effectively capitalize on charging during low-price periods and discharging during high-price intervals.

5.2 Cost Breakdown Analysis

To further examine the cost structure in detail, a comprehensive breakdown of each cost component for all scenarios is depicted in Fig. 3. Across all case studies, electricity purchased from the grid constitutes the most significant portion of the total cost, accounting for approximately 88%, 100%, 89%, and 94% in Cases 1 through 4, respectively. CO_2 emission cost is considered proportional to the electricity consumption, as in Sweden most of the electricity is generated from renewable energies, this share is around 1.7% of the total cost, which can be neglected. It can also be seen that the peak power surcharge in Case 4 is the lowest among all cases, while Case 1 shows the highest. Additionally, investment costs for PV installations represent the most significant capital expenditure in Cases 2 and 4, while the battery investment costs in Cases 3 and 4 account for a smaller proportion compared to the electricity consumption costs. In Case 2 and Case 4, PV installation enables electricity sales back to the grid, which appears as negative cost components, contributing to 61% and 60% of total costs, respectively. These revenues substantially offset the net electricity expenses and play a crucial role in reducing the overall cost and increasing the self-sufficiency rate. Furthermore, without PV, Cases 1 and 3 do not generate grid export revenue.

To further investigate the impact of energy configurations on peak power charges, the monthly peak power imported from the power grid is illustrated in Fig. 4(a), with the corresponding percentage reductions shown in Fig. 4(b). Compared to Case 1, the monthly peak power imports exhibit noticeable reductions when PV, battery, or combination are incorporated in Cases 2 to 4. Specifically, Case 4 demonstrates the most substantial reductions, achieving peak power decreasing to approximately 380 kW during summer months and about 919 kW in winter months. Consequently, the monthly peak power reduction

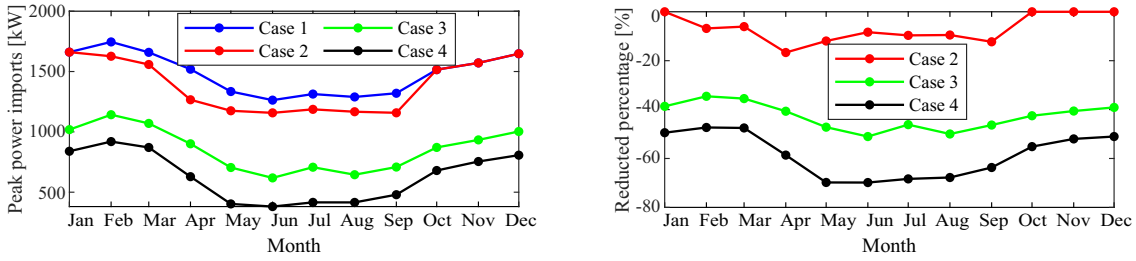

Figure 4: Comparison of monthly peak power imported from the grid for **(a)**: absolute values per month and **(b)**: relative reduction compared to Case 1.

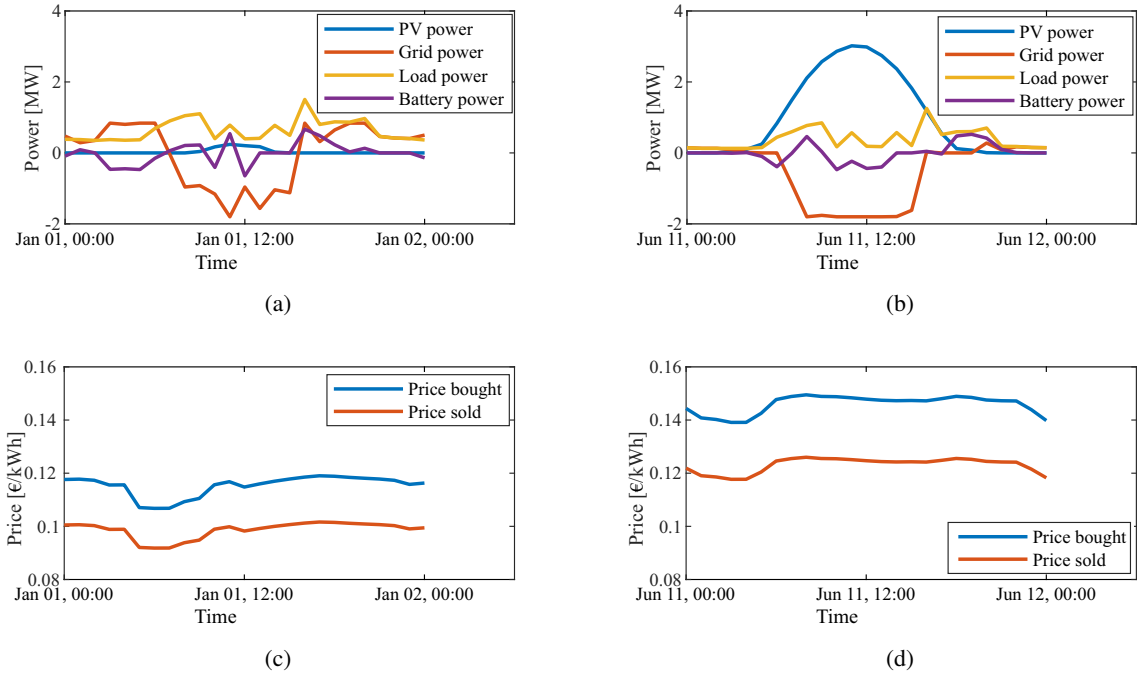

Figure 5: Example daily power profiles of **(a)**: winter day, **(b)**: summer day, and associated electricity prices (**c**): winter day and (**d**): summer day.

percentages range between 51% and 69% compared to Case 1, highlighting the effectiveness of combined PV and battery systems in minimizing peak power demand.

In contrast, Case 3, featuring only battery storage, displays a similar trend in peak power imports and reduction percentages to Case 4, attributable to the battery capability for bidirectional power management, shifting consumption patterns effectively. However, Case 2, which involves only PV installation, results in relatively minor reductions in peak power imports, with most monthly reductions less than 20% compared to Case 1. This observation suggests limited peak-shaving capability when only PV is used.

5.3 Power Allocations in Case 4

Given that Case 4 demonstrates the lowest total cost, the power distribution among system components is further analyzed. Fig. 5(a) and Fig. 5(b) illustrate daily power profiles for grid supply, PV generation, battery operation, and total load demand during representative winter and summer days. For clarity, corresponding electricity prices for purchasing and selling are shown in Fig. 5(c) and Fig. 5(d). Significant seasonal variations in PV generation are evident, with a peak value of 3 MW in summer and 1 MW in winter, influencing grid behavior substantially. Due to insufficient PV generation in winter, the power grid primarily supplies the load demand during early morning, late evening, and nighttime periods. Additionally, negative grid power values between 10 AM and 1 PM indicate electricity sold back to the

grid, and battery charging at approximately 6 AM aligns with low electricity purchase prices, taking advantage of the higher selling price at midday. Conversely, during summer, PV generation exceeds load demand significantly, and surplus electricity is sold back to the grid, generating revenue. In summer, battery activity involves relatively minor power exchanges, approximately 0.48 MW for discharging and -0.47 MW for charging.

6 Conclusion and Discussion

To evaluate the techno-economics of PV and battery, the paper introduces a co-design energy system optimization framework for an airport microgrid to determine optimal sizes for PV and BESS across four distinct scenarios. Additionally, the framework optimizes power allocation between PV and BESS to minimize operational and investment costs. The comparative analysis shows that integrating PV and BESS systems achieves the best cost performance, significantly reducing total electricity costs and peak power surcharges. For the optimal PV and BESS sizing in Case 4, a 46% cost reduction is achieved compared to the reference case (Case 1) without any additional investments.

Acknowledgments

The authors would like to express their gratitude to the Swedish Transport Agency for its financial support through the project *Elflyg i Sverige (ELFLYSVE)* through the grant number of TRV 2023/34443.

References

[1] Statista, "Environmental impact of the aviation industry worldwide - statistics & facts," Available at https://www.statista.com/topics/7346/environmental-impact-of-the-aviation-industry-worldwide/#topicOverview (2024/04/16).

[2] A. D. Cristea, "The role of aviation networks for urban development," *Journal of Regional Science*, vol. 63, no. 4, pp. 947–980, 2023.

[3] S. L. B. Santa, J. M. P. Ribeiro, G. Mazon, J. Schneider, R. L. Barcelos, J. B. S. O. de Andrade *et al.*, "A green airport model: Proposition based on social and environmental management systems," *Sustainable Cities and Society*, vol. 59, p. 102160, 2020.

[4] International Airport Review, "Rome Fiumicino airport unveils europe's largest self-consumption solar farm to boost sustainability efforts," Available at https://www.internationalairportreview.com/news/233878/rome-fiumicino-airport-unveils-europes-largest-self-consumption-solar-farm-to-boost-sustainability-efforts/ (2025/01/21).

[5] PV Europe, "Enercity builds solar plant on the premises of German airport," Available at https://www.pveurope.eu/installation/hanover-airport-enercity-builds-solar-plant-premises-german-airport (2024/11/21).

[6] M. Jiang, L. Qi, Z. Yu, D. Wu, P. Si, P. Li, W. Wei, X. Yu, and J. Yan, "National level assessment of using existing airport infrastructures for photovoltaic deployment," *Applied Energy*, vol. 298, p. 117195, 2021.

[7] A. Ficca, F. Marulo, and A. Sollo, "An open thinking for a vision on sustainable green aviation," *Progress in Aerospace Sciences*, vol. 141, p. 100928, 2023.

[8] C. Y. Justin, A. P. Payan, S. I. Briceno, B. J. German, and D. N. Mavris, "Power optimized battery swap and recharge strategies for electric aircraft operations," *Transportation Research Part C: Emerging Technologies*, vol. 115, p. 102605, 2020.

[9] J. Hellgren, M. Persson, and H. Alfredsson, "Airport charging system designs and power management for megawatt-level charging of battery-electric aircraft," in *34th Congress of the International Council of the Aeronautical Sciences, ICAS 2024. Florence, Italy. 9 September 2024 through 13 September 2024*. International Council of the Aeronautical Sciences, 2024.

[10] P. Ollas, S. G. Sigarchian, H. Alfredsson, J. Leijon, J. S. Döhler, C. Aalhuizen, T. Thiringer, and K. Thomas, "Evaluating the role of solar photovoltaic and battery storage in supporting electric aviation and vehicle infrastructure at Visby airport," *Applied Energy*, vol. 352, p. 121946, 2023.

[11] Copenhagen Airports A/S, "Copenhagen airport installs large battery for green energy storage," Available at https://www.cph.dk/en/about-cph/press/news/2024/03/copenhagen%20airport%20installs%20large%20battery%20for-%20green%20energy%20storage (2024/03/20).

[12] Schiphol, "Super battery being tested at schiphol: a world first at the airport," Available at https://news.schiphol.com/super-battery-being-tested-at-schiphol-a-world-first-at-the-airport/? (2024/06/26).

[13] A. Micallef, J. M. Guerrero, and J. C. Vasquez, "New horizons for microgrids: From rural electrification to space applications," *Energies*, vol. 16, no. 4, p. 1966, 2023.

[14] Y. Xiang, H. Cai, J. Liu, and X. Zhang, "Techno-economic design of energy systems for airport electrification: A hydrogen-solar-storage integrated microgrid solution," *Applied Energy*, vol. 283, p. 116374, 2021.

[15] Z. Guo, B. Li, G. Taylor, and X. Zhang, "Infrastructure planning for airport microgrid integrated with electric aircraft and parking lot electric vehicles," *eTransportation*, vol. 17, p. 100257, 2023.

[16] H. Zhao, Y. Xiang, Y. Shen, Y. Guo, P. Xue, W. Sun, H. Cai, C. Gu, and J. Liu, "Resilience assessment of hydrogen-integrated energy system for airport electrification," *IEEE Transactions on Industry Applications*, vol. 58, no. 2, pp. 2812–2824, 2021.

[17] P. Ollas, J. Persson, and K. Peter, "Effect of energy storage on self-consumption and self-sufficiency: A field study in a nordic climate," in *Proceedings of the 38th European Photovoltaic Solar Energy Conference and Exhibition, Online*, 2021, pp. 6–10.

[18] A. Stephan, B. Battke, M. D. Beuse, J. H. Clausdeinken, and T. S. Schmidt, "Limiting the public cost of stationary battery deployment by combining applications," *Nature Energy*, vol. 1, no. 7, pp. 1–9, 2016.

[19] W. Durisch, B. Bitnar, J.-C. Mayor, H. Kiess, K. hang Lam, and J. Close, "Efficiency model for photovoltaic modules and demonstration of its application to energy yield estimation," *Solar Energy Materials and Solar Cells*, vol. 91, no. 1, pp. 79–84, 2007.

[20] D. L. King, W. E. Boyson, and J. A. Kratochvil, "Photovoltaic array performance model," Sandia National Laboratories, Albuquerque, NM, USA, Technical Report SAND2004-3535, 2004, accessed: Mar. 2025. [Online]. Available: https://prod-ng.sandia.gov/techlib-noauth/access-control.cgi/2004/043535.pdf

[21] Q. Xun, M. Langwasser, F. Gao, and M. Liserre, "Optimal sizing and energy management of smart-transformer-based energy storage systems for residential communities," in *2023 IEEE 14th International Symposium on Power Electronics for Distributed Generation Systems (PEDG)*, 2023, pp. 891–896.

[22] H. Alfredsson, J. Nyman, J. Nilsson, and I. Staack, "Infrastructure modeling for large-scale introduction of electric aviation," in *35th International Electric Vehicle Symposium and Exhibition (EVS35) Oslo, Norway, June 11-15, 2022*, 2022.

[23] Q. Xun, N. Murgovski, and Y. Liu, "Chance-constrained robust co-design optimization for fuel cell hybrid electric trucks," *Applied Energy*, vol. 320, p. 119252, 2022.

[24] Government Offices of Sweden. (2025) Sweden's carbon tax. [Online]. Available: https://www.government.se/government-policy/taxes-and-tariffs/swedens-carbon-tax/

[25] Nowtricity. (2025) Historical data for sweden. [Online]. Available: https://www.nowtricity.com/country/sweden/

Presenter Biography

Qian Xun received her Ph.D. in Electric Power Engineering from the Chalmers University of Technology, Sweden, in 2022. She is currently a Senior Researcher at the Unit of Energy Conversion, RISE Research Institutes of Sweden, Sweden. She was previously a Research Fellow at the Center of Electronic Energy Systems, Fraunhofer Institute for Silicon Technology ISIT, Germany. Her research focuses on modeling, control, and optimization of hydrogen energy storage systems for automotive and microgrid applications, power electronics, motion control, and wide band-gap devices.